CHAPTER IV
SYNTHESIS AND CHARACTERIZATION OF NR/HMS COMPOSITES

In this Chapter, mesoporous silica composite based on natural rubber (NR) and hexagonal mesoporous silica (HMS) was studied. This material was prepared via an *in situ* sol-gel process. Unlike the conventional procedure for HMS synthesis, in this work tetrahydrofuran (THF) was used as synthesis media instead of ethanol to thoroughly dissolve the NR in the synthesis mixture and to obtain a high dispersion level of the NR in the silica framework. Using dodecylamine (DDA) as the organic template, the effects of molar composition of TEOS: H_2O: DDA on the physicochemical properties of the NR/HMS composites obtained were investigated as described in Chapter III. The composites obtained possessed a highly ordered hexagonal mesostructure and textural properties concomitantly with their enhanced hydrophobicity.

4.1 Thermogravimetric analysis (TGA)

Figure 4.1 shows TG and DTG curves of NR/HMS-1, as a representative sample of all the other NR/HMS samples to determine the amount of NR in the composites, compared with those of pure NR. As revealed in Figure 4.1, the weight loss of NR/HMS occurred between 40 and 150 °C was due to evaporation of physisorbed water (5-8 wt.%). The second major weight loss (12-14 wt.%) of the composite in the temperature range from 200 to 440 °C should be attributed to the decomposition of NR as suggested by the TGA result of pure NR (Figure 4.2)). The small weight loss in the range of 450-650 °C was related to carbon residue derived from the NR decomposed on the composite structure and condensation of silanol groups. The silica content of the NR/HMS composite was determined from the weight remaining at the temperature of 1,000 °C. In the typical synthesis conditions, the silica content was around 75-79 wt.% as summarized in Table 4.1.

Table 4.1 Silica content of NR/HMS composites synthesized under various conditions.

Sample[a]	Molar composition (mol%)						Silica content[b] (%)
	TEOS	DDA	H_2O	NR	Ethanol	THF	
NR/HMS-1	0.1	0.03	2.94	0.01	-	0.37	77.3
NR/HMS-2	0.1	0.03	4.42	0.01	-	0.37	77.8
NR/HMS-3	0.1	0.03	5.89	0.01	-	0.37	77.3
NR/HMS-4	0.1	0.04	2.94	0.01	-	0.37	76.6
NR/HMS-5	0.1	0.05	2.94	0.01	-	0.37	75.4
NR/HMS-6	0.1	0.07	2.94	0.01	-	0.37	75.5
NR/HMS-7	0.1	0.03	2.94	0.02	-	0.74	69.2
NR/HMS-8	0.1	0.04	5.89	0.01	-	0.37	78.5

n.d. = not determined.

[a] Extracted samples.

[b] Determined by thermogravimetric analysis.

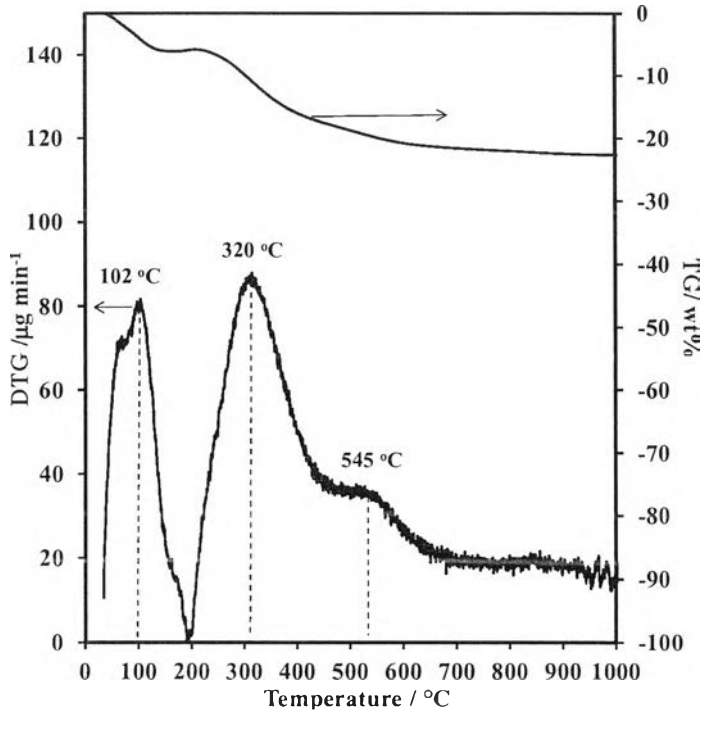

Figure 4.1 Weight loss and DTG curves of NR/HMS-1 composite.

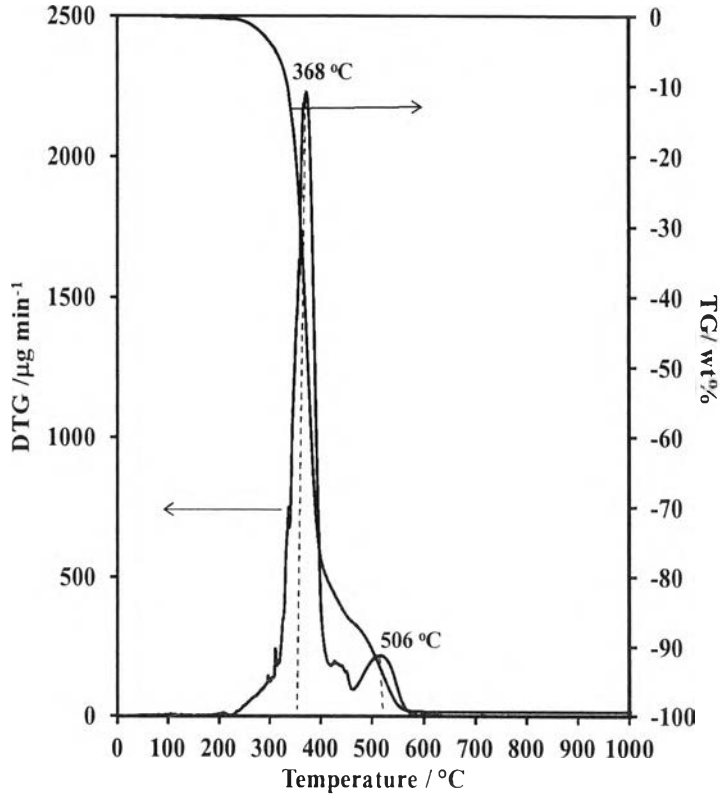

Figure 4.2 Weight loss and DTG curves of pure NR.

4.2 FTIR spectroscopy

The FTIR spectroscopy was used to confirm the presence of NR in the HMS structure. As shown in Figure 4.3, the main bands of pure mesoporous silicas (HMS-E and HMS-T) and NR/HMS composite were observed between 1000 and 1300 cm^{-1}, which represented the Si–O–Si stretching of the silica framework. Both of pure silica HMSs exhibited very intense band at 3760 cm^{-1} relating to free silanol groups (Si-OH). In addition, the bands locating at 3030, 2962, 2924, 2850, 1660, 1450 and 1378 cm^{-1} were found for NR/HMS-1, all of which corresponds to the characteristics of the NR structure [100, 101]. It can be seen that NR/HMS composite lowered the absorbance of free silanol band. Moreover, NR/HMS-1 gave a broad band of hydrogen-bonded silanol groups around 3500 cm^{-1}. These results implied that the surface of HMS was covered with the NR molecules.

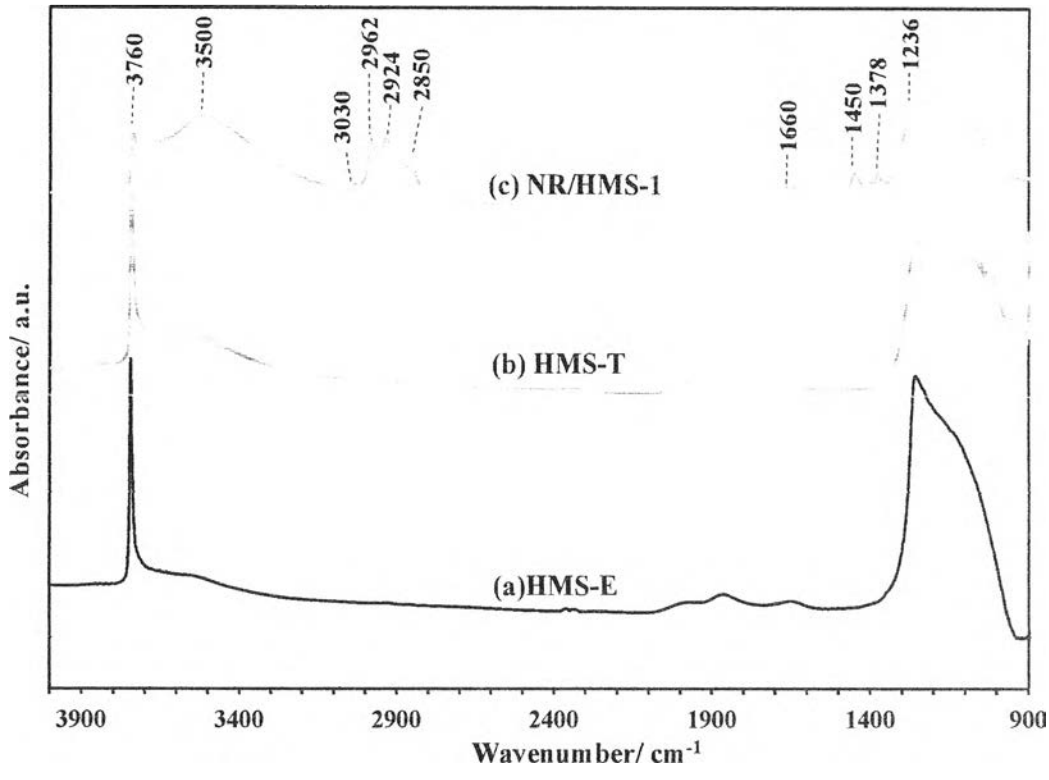

Figure 4.3 FTIR spectra of mesoporous silica (a) HMS-E, (b) HMS-T and (c) NR/HMS-1 composite.

4.3 Solid state ^{29}Si MAS NMR studies

Figure 4.4 shows ^{29}Si MAS NMR of pure silica HMS-T and NR/HMS-1, as a representative sample of the NR/HMS composites. By comparing the intensities of Q^n groups of these materials in Table 4.2, the NR/HMS-1 composite revealed lower relative intensity of Q^2 and Q^3 than pure silica HMS-T, while the higher relative intensity of Q^4 was observed for NR/HMS-1 composite was observed. These results suggested that the formation of NR/HMS composite reduced the amount of surface silanol groups in accordance with the FTIR results as shown in Figure 4.3.

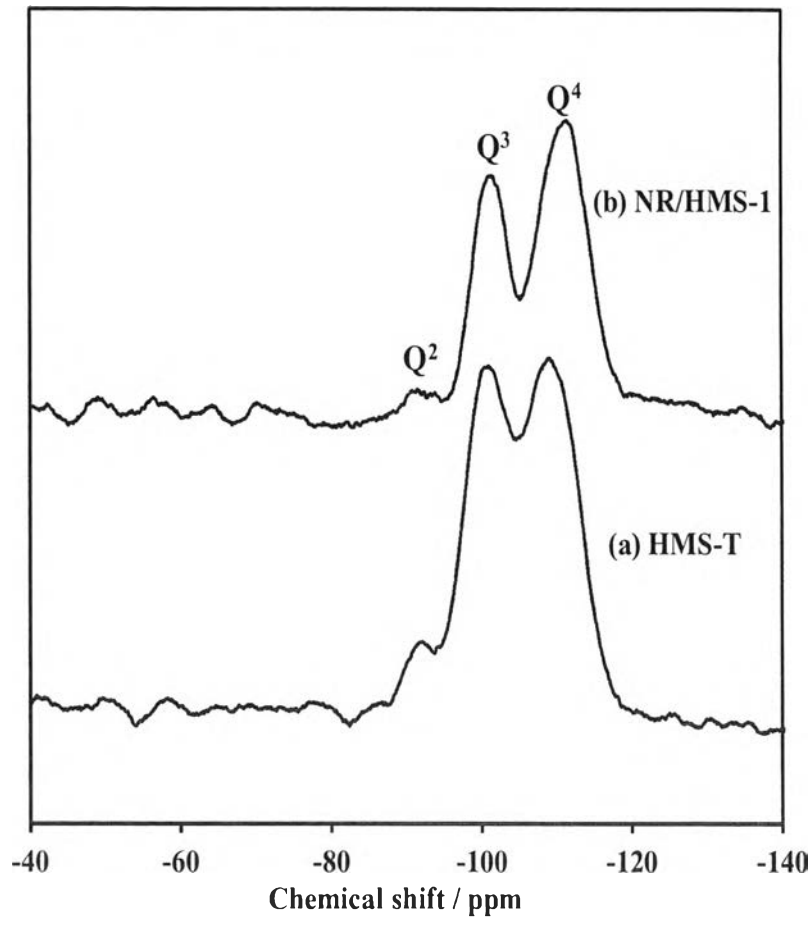

Figure 4.4 ^{29}Si MAS NMR spectra of (a) HMS-T and (b) NR/HMS-1 composite.

Table 4.2 Relative intensity of the Q^n group (obtained from the deconvolution of the ^{29}Si MAS NMR by using Origin Professional software (version 8.5)).

Sample	Relative intensity		
	Q^2 (%) 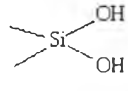	Q^3 (%) 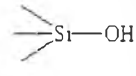	Q^4 (%) 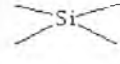
a) HMS-T	5.9	40.3	53.8
b) NR/HMS-1	3.4	34.4	62.3

4.4 XRD analysis

The XRD patterns of the pure silica HMSs and the NR/HMS composites after the extraction of template molecules are shown in Figures 4.5 and 4.6, respectively. The pure silica HMS samples prepared in ethanol and THF exhibited strong diffraction peak of (100) plane at 2-Theta in the range of 1.0-3.0 ° (Figure 4.5). The lower 2-Theta position of the peak observed for HMS-T, when compared to that of HMS-E, corresponded to an increase in the d_{100} spacing and unit cell parameter of hexagonal mesostructure as summarized in Table 4.3. It should be related to lower polarity of THF as the synthesis media that can expand the DDA molecules, resulting in an enlargement of hexagonal array of micellar rods. In addition, HMS-T exhibited higher wall thickness than HMS-E. These characteristics may afford superior thermal and hydrothermal stability to the conventional HMS.

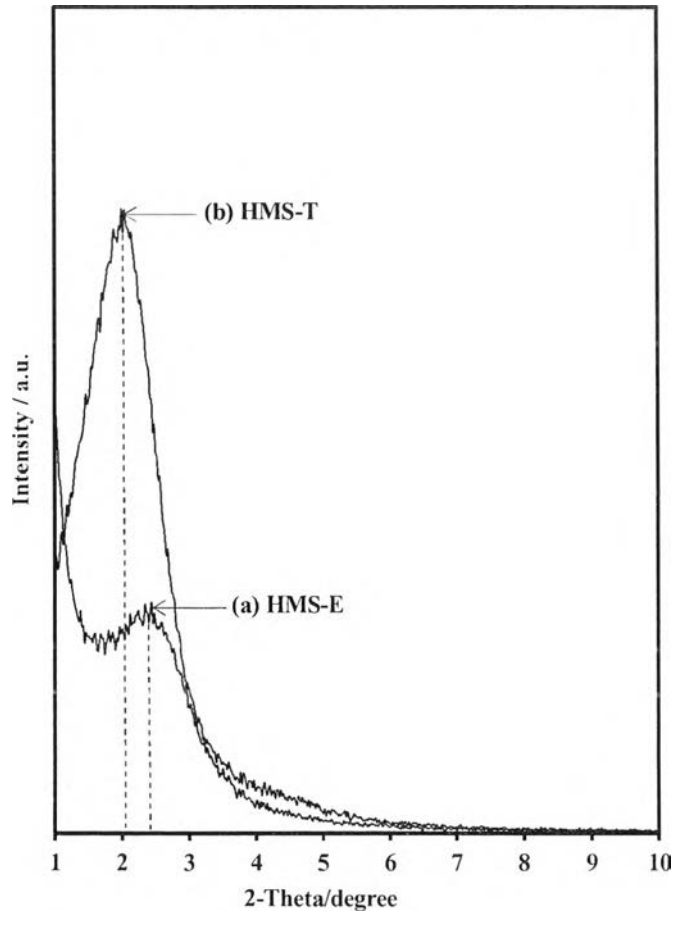

Figure 4.5 XRD patterns of (a) pure silica HMS-E and (b) pure silica HMS-T after extractive removal the DDA template prior to the analysis.

Table 4.3 Structural properties of pure silica HMSs and NR/HMS composites synthesized under various conditions.

Sample[a]	Molar composition (mol%)						d_{100}[b] (nm)	a_0[c] (nm)	W_T[d] (nm)
	TEOS	DDA	H_2O	NR	Ethanol	THF			
HMS-E	0.1	0.03	2.94	-	0.08	-	3.5	4.0	1.9
HMS-T	0.1	0.03	2.94	-	-	0.37	4.4	5.0	2.2
NR/HMS-1	0.1	0.03	2.94	0.01	-	0.37	4.9	5.7	3.0
NR/HMS-2	0.1	0.03	4.42	0.01	-	0.37	4.7	5.5	2.7
NR/HMS-3	0.1	0.03	5.89	0.01	-	0.37	5.0	5.7	2.9
NR/HMS-4	0.1	0.04	2.94	0.01	-	0.37	5.0	5.8	3.0
NR/HMS-5	0.1	0.05	2.94	0.01	-	0.37	4.7	5.4	2.4
NR/HMS-6	0.1	0.07	2.94	0.01	-	0.37	4.9	5.7	2.9
NR/HMS-7	0.1	0.03	2.94	0.02	-	0.74	5.1	5.9	3.7
NR/HMS-8	0.1	0.04	5.89	0.01	-	0.37	4.9	5.7	2.5

n.d. = not determined.

[a] Extracted samples.

[b] d_{100} from XRD analysis.

[c] The repeat distance (a_0) between pore centers of the hexagonal structure was calculated from $a_0 = 2d_{100} / 3^{1/2}$.

[d] The framework wall thickness was determined by subtracting the BJH mesopore size from the repeat distance between pore centers.

As shown in Figure 4.6, the characteristic peaks of all NR/HMS composites were shifted to lower 2-Theta than that of HMS-T, indicating that the unit cell of HMS was enlarged by the addition of NR as summarized in Table 4.3. These results suggested that the NR molecules were incorporated into the hexagonal mesostructure of HMS by which the wall thickness of NR/HMS was significantly increased. The presence of NR in the HMS structure also affected hexagonally ordering of mesoporous channels in different manners, depending on the molar composition of the synthesis mixture as evidenced by the XRD peak intensity.

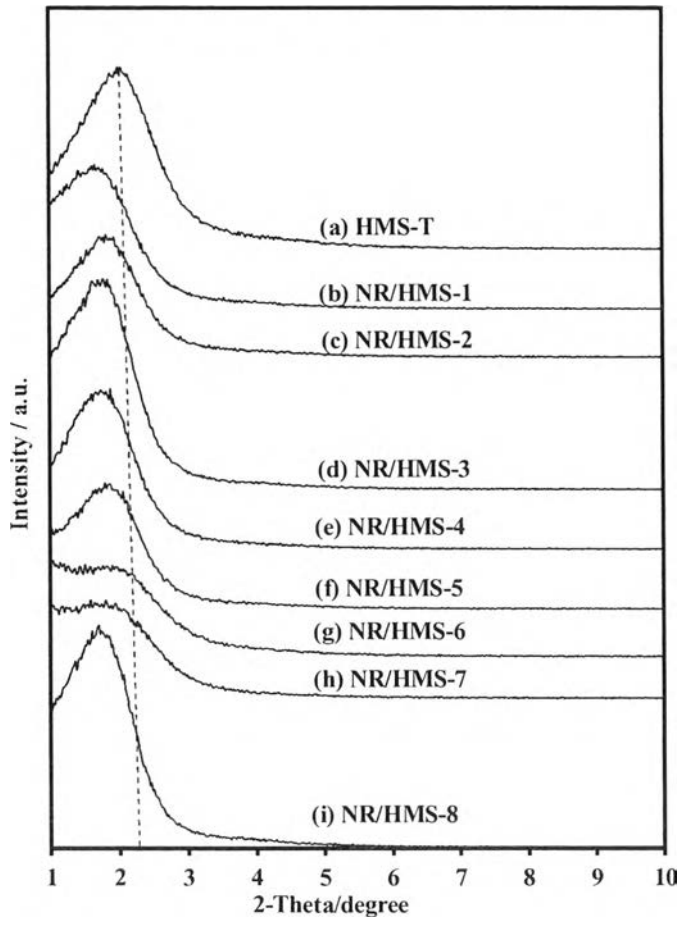

Figure 4.6 XRD patterns of (a) pure silica HMS-T and (b-i) NR/HMS composites after extractive removal of the DDA template prior to the analysis.

With increasing the amount of H_2O (from NR/HMS-1 to NR/HMS-3), the characteristic peak was increased in the intensity, indicating an improved hexagonal packing of mesoporous channels. It should be due to promotion of the silica source hydrolysis to silicate species by the increased amount of H_2O.

When the amount of DDA was increased (from NR/HMS-4 to NR/HMS-6), a detrimental effect on the HMS structure was observed as evidenced by the broad and low intensity peaks. On one hand, the hydrolysis of silica source and the condensation of silicate species were encouraged at high DDA concentration since the pH of synthesis mixture was increased. The precipitation of silica under such a condition was very fast, leading to less ordered mesoporous structure. On the other hand, the excess DDA molecules could modify the solubility of NR in the THF/H_2O

mixture and around the silicate layers. Similarly to the effect of DDA, increasing NR loading lowered the hexagonal ordering as seen from a decrease in the XRD peak intensity (NR/HMS-7). However, the composite with highly order mesoporous structure can be achieved by properly increasing both the H_2O and DDA amount (NR/HMS-8). By comparing with the structural data obtained from HMS-T as summarized in Table 4.3, the expansion of unit cell simultaneously with thicken wall observed for the NR/HMS composites suggested that NR should be incorporated into the mesopore walls between which the channels were arranged in the hexagonal manner, since the molecular size of NR is too large to accommodate inside the primary mesoporosity.

4.5 Transmission electron microscopy (TEM)

Figures 4.7-4.9 show the TEM images of HMS-E, HMS-T and NR/HMS-1 composite as representative sample, respectively. These materials exhibited uniform framework-confined mesoporous channels of wormhole-like structure. From analyzing TEM images with a FamtoScan program in 2D and 3D mode, the black color represents the mesoporous channels and the bright orange/white color represents the silica wall. It can be clearly seen that the HMS synthesized in THF (HMS-T) exhibited larger pore diameter and thicker wall than the conventional that synthesize in Ethanol. This result was in accordance with the data on the wall thickness data (Table 4.3). In the case of NR/HMS-1 composite, the white area was found to be increased, while the number of black spots was decreased (Figure 4.9). Further, the estimated ratio of the number of pore channels per unit area observed for these samples was in the following order: HMS-E (0.015) > HMS-T (0.013) > NR/HMS-1 (0.009). By measuring the wall thickness of mesopore channel on the simulated 2D images as illustrated in Figure 4.10, the average wall thickness of NR/HMS-1 composite (~3.1 nm) was higher than that of pure silica HMS-T (~2.4 nm). These results corresponded with the estimated wall thickness as summarized in Table 4.3.

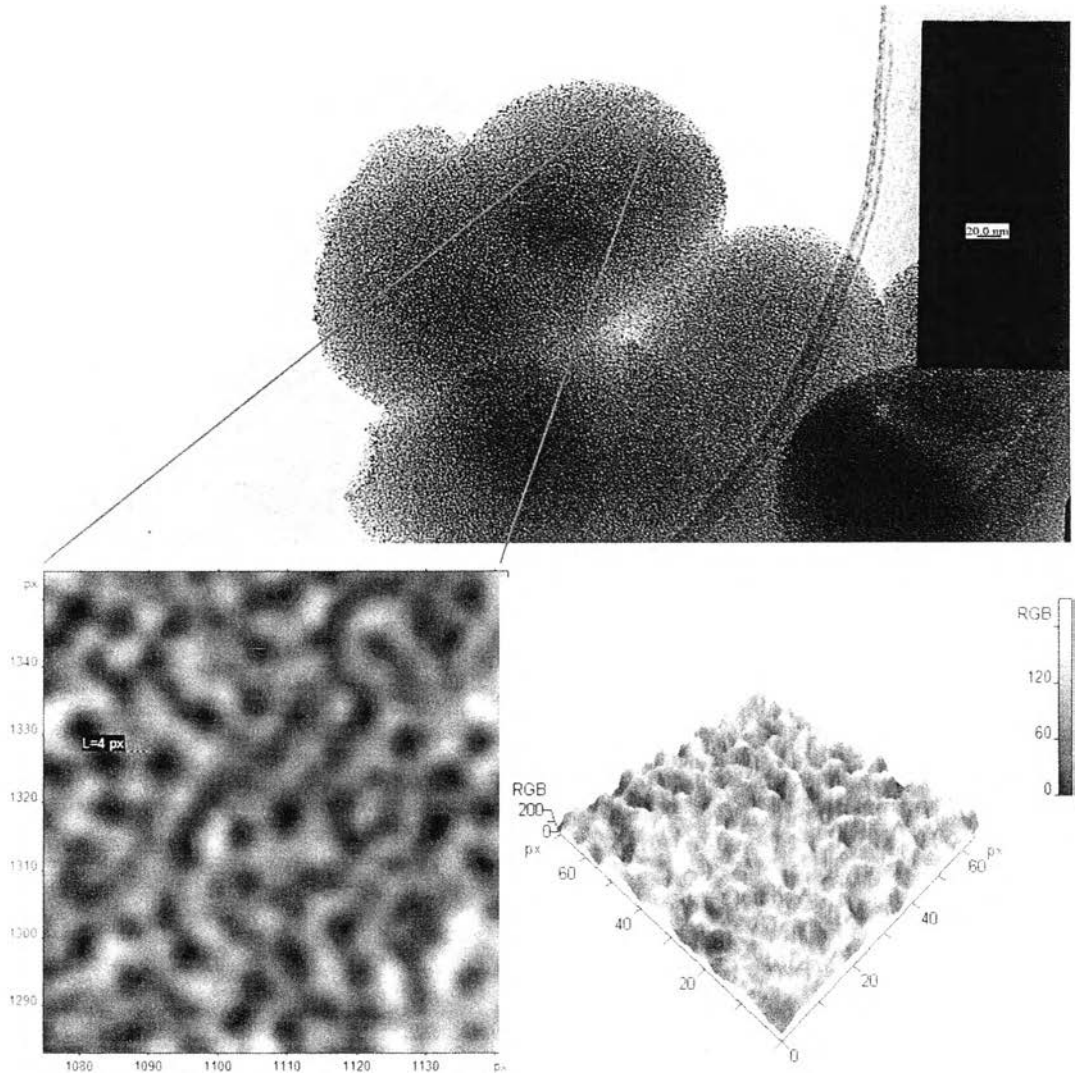

Figure 4.7 TEM images and the simulated 2D and 3D TEM images of HMS-E.

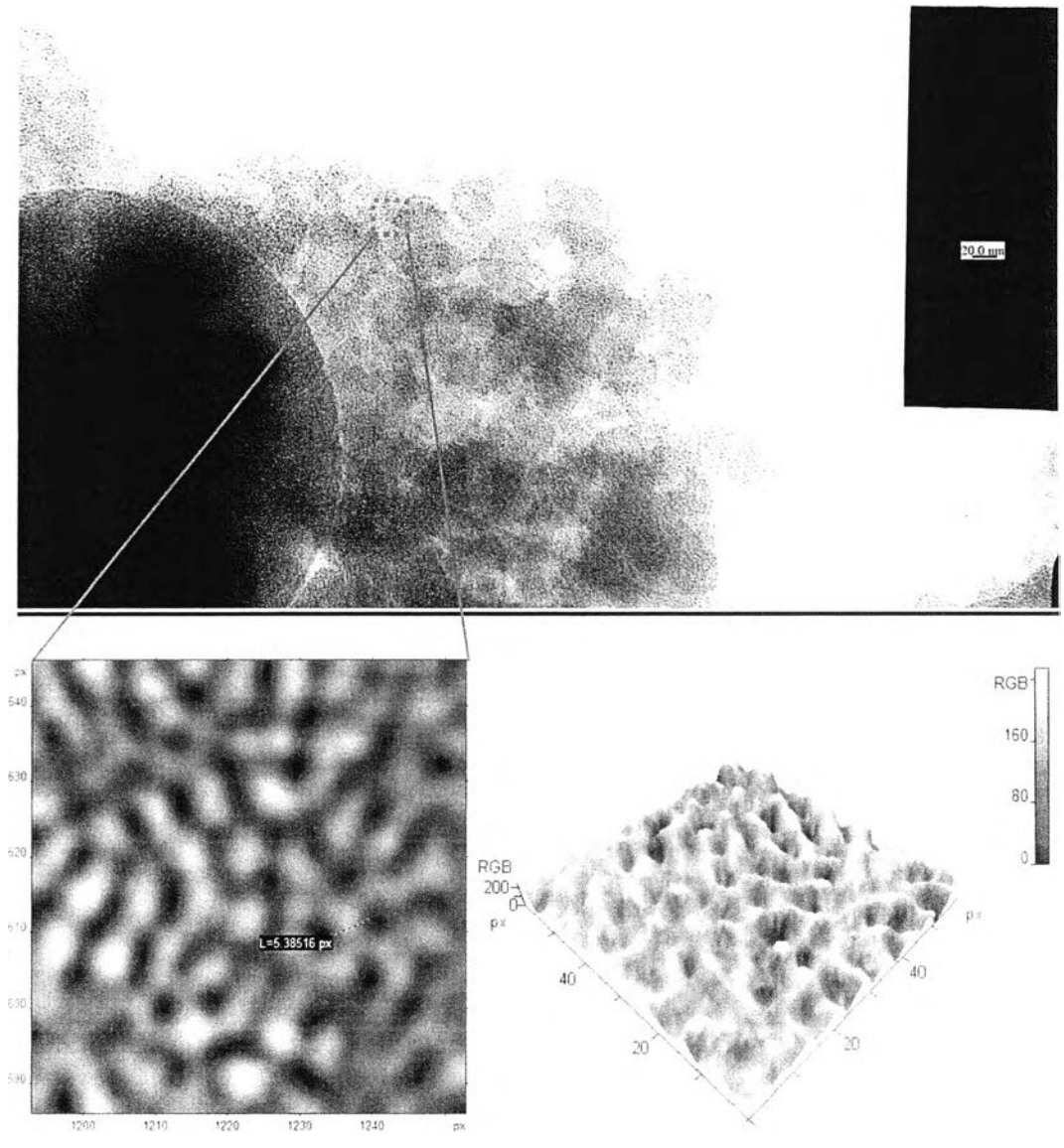

Figure 4.8 TEM image and the simulated 2D and 3D TEM images of HMS-T.

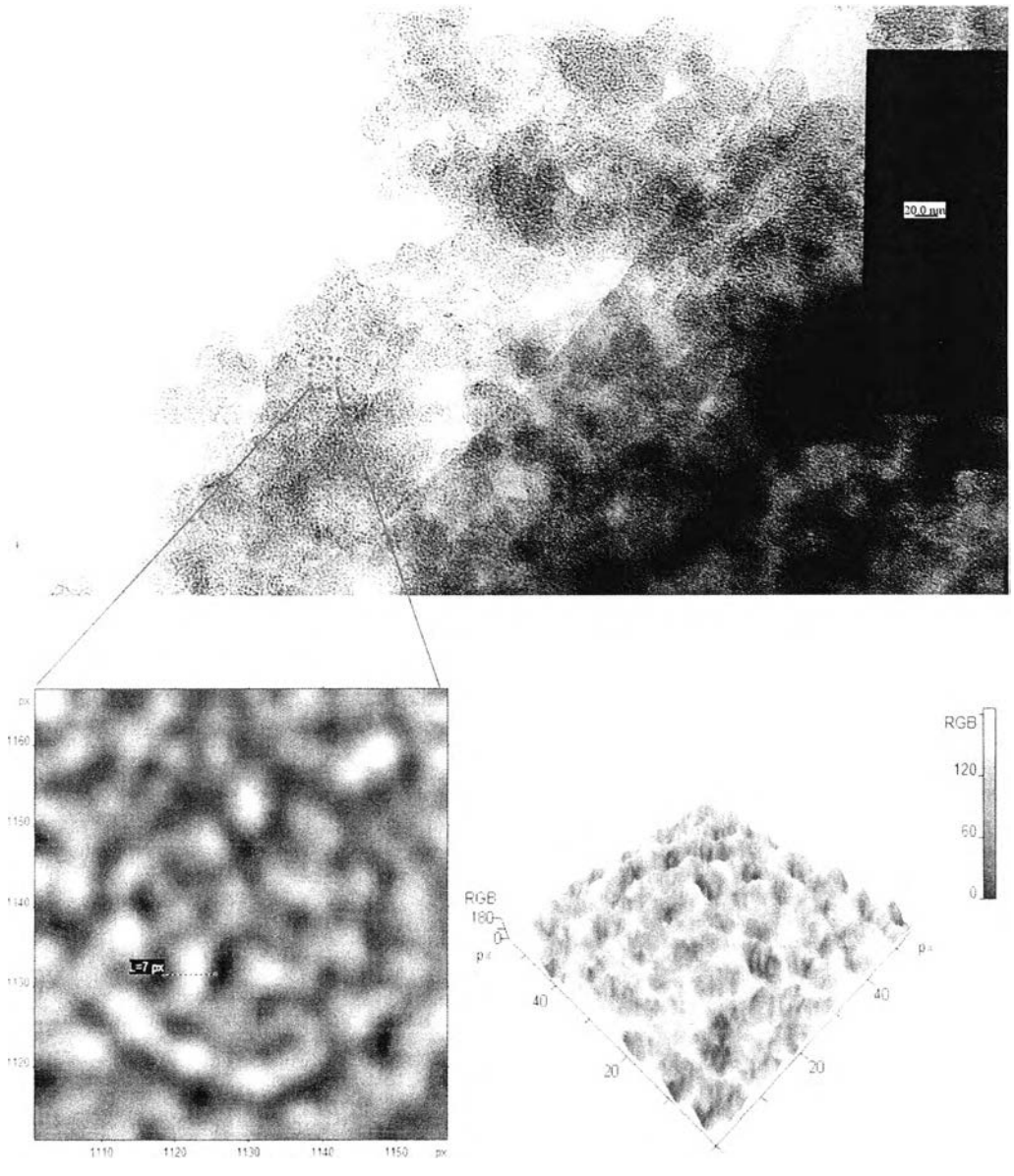

Figure 4.9 TEM image and the simulated 2D and 3D TEM images of NR/HMS-1 composite.

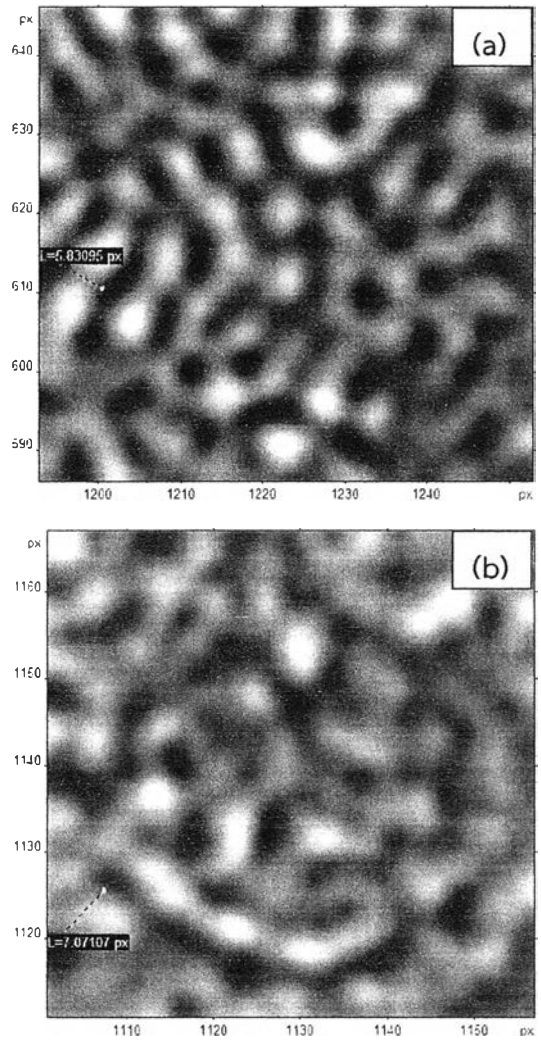

Figure 4.10 Simulated 2D TEM images of (a) HMS-T and (b) NR/HMS-1 composite; the distance of 20 nm was equivalent to 45 pixels. The data reported were average values of 20 different measured areas.

4.6 Scanning electron microscopy (SEM)

The morphology of NR/HMS-1 composite, compared with that of HMS-T, is revealed by the FE-SEM images in Figures 4.11 and 4.12. HMS-T exhibited small spherical aggregates of silica particles that were homogeneously dispersed in the agglomerates as shown in Figures 4.11(a) and (b). The presence of NR in HMS structure (NR/HMS-1 composite) enhanced the agglomeration of HMS particles as shown in Figures 4.12(a) and (b).

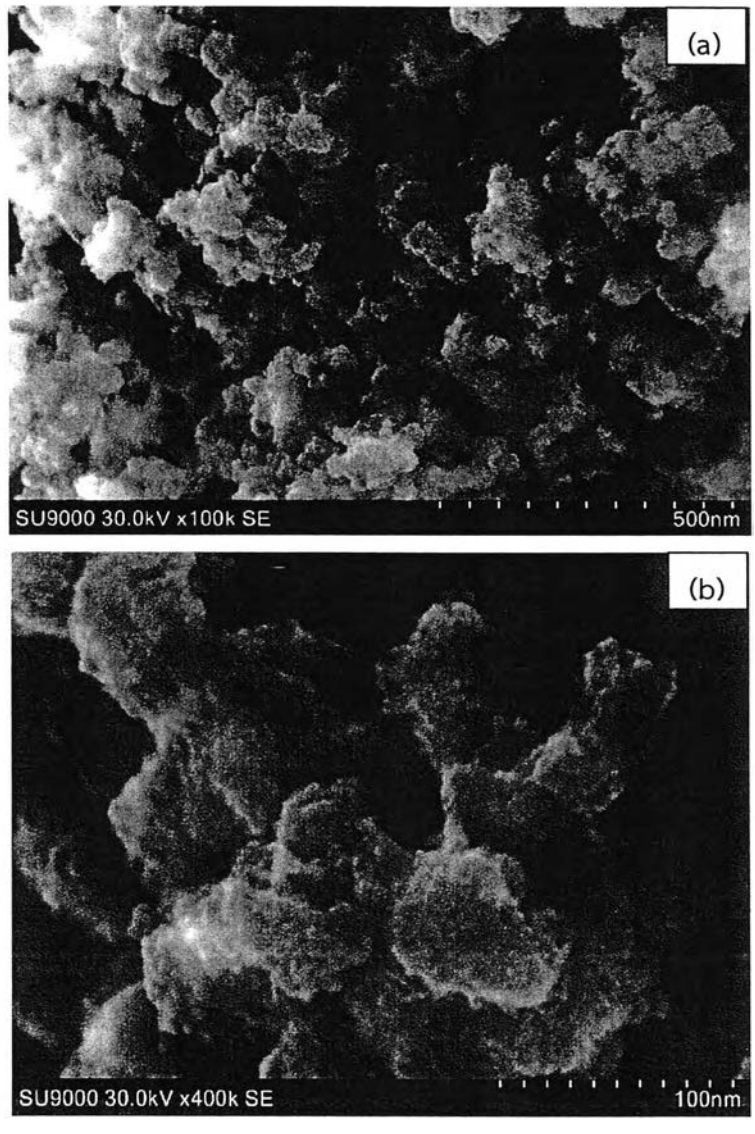

Figure 4.11 FE-SEM images at a magnification of (a) x100,000 and (b) x400,000 of HMS-T.

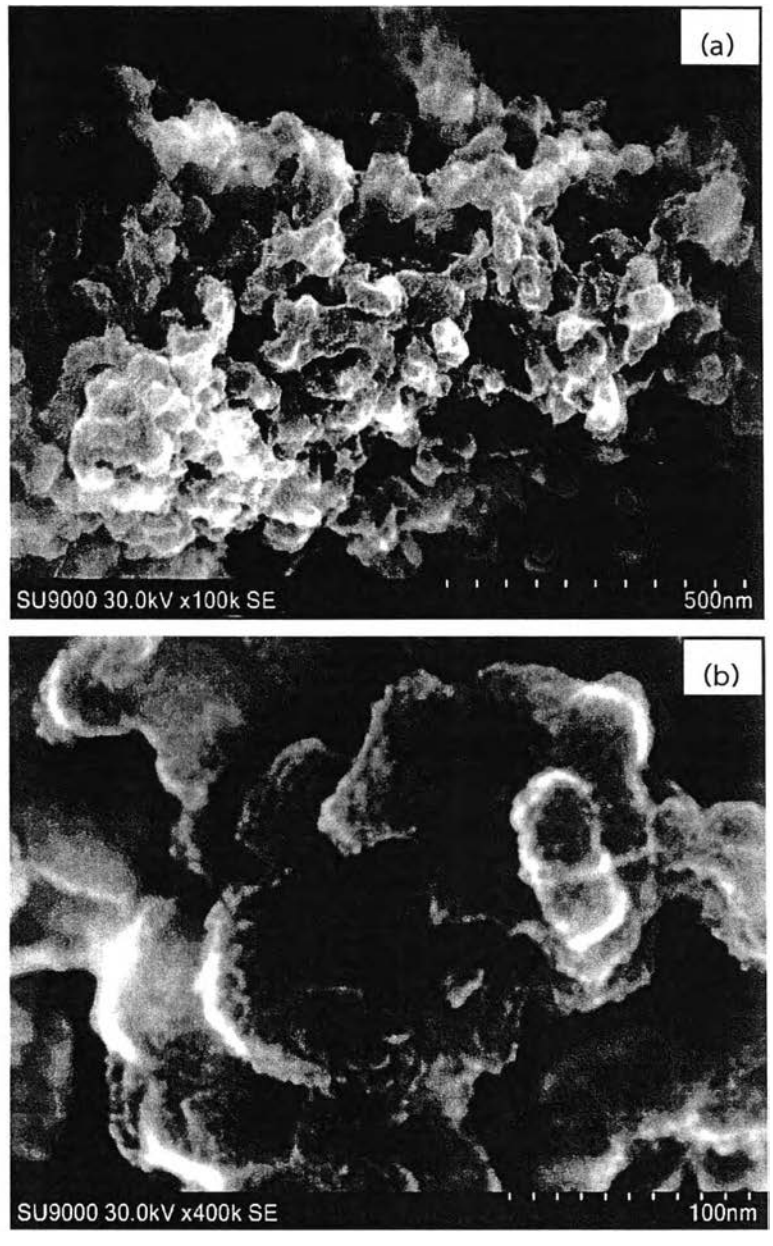

Figure 4.12 FE-SEM images at a magnification of (a) x100,000 and (b) x400,000 of NR/HMS-1 composite.

4.7 Particle size analysis

The particle size distribution of HMS-T compared with that of NR/HMS-1 composite are shown in Figure 4.13. The pure silica HMS-T revealed a unimodal size distribution with particle sizes in the range 0.98-2.0 nm. The presence of NR in HMS structure (NR/HMS-1 composite) resulted in an increase in the mean size of the NR/HMS agglomerates to 79.4 nm as shown in Figure 4.13(b). These result related to their FE-SEM images.

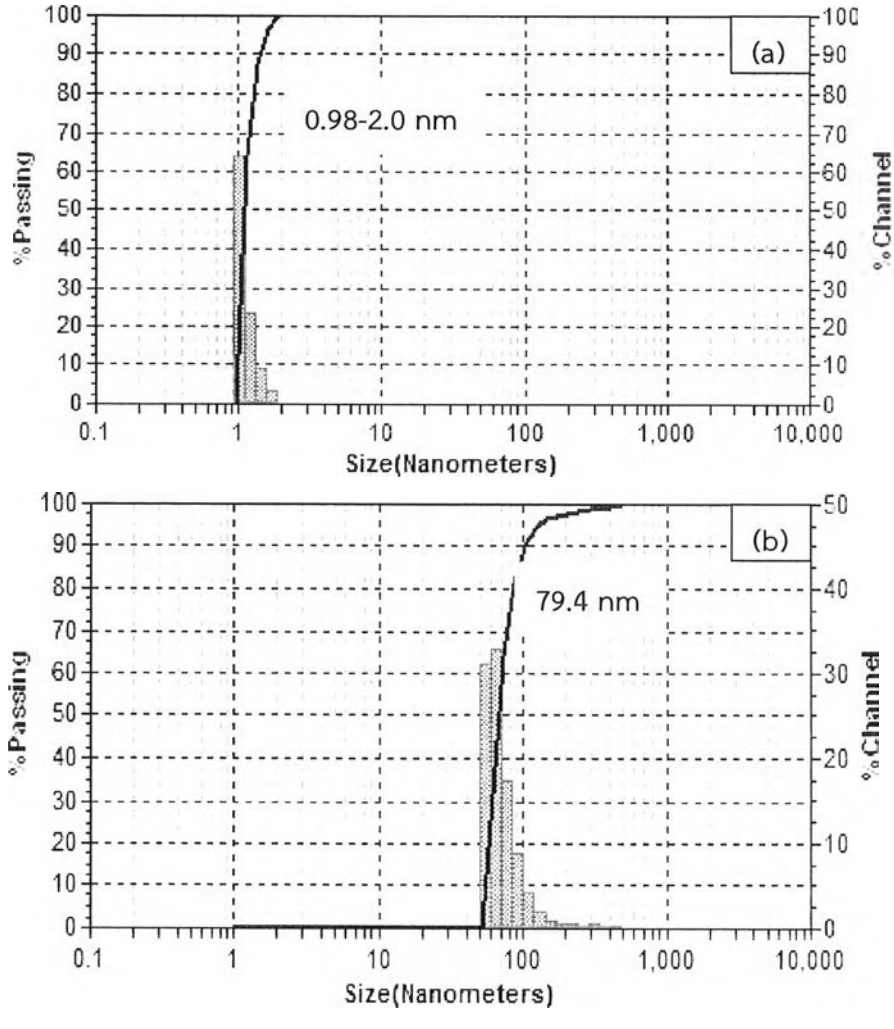

Figure 4.13 Particle size distribution of the (a) pure silica HMS-T, and (b) NR/HMS-1 composite.

4.8 N_2 adsorption-desorption measurement

The N_2 adsorption-desorption isotherms and BJH pore size distribution of HMS-E and HMS-T are shown in Figure 4.14. The HMSs prepared in ethanol and THF exhibited the shape of sorption isotherms as type IV, according to the IUPAC classification, with the hysteresis loops at the relative pressure (P/P_0) ranging from 0.2-0.4, which is the characteristics of framework confined mesoporous materials (Figure 4.14(a)). More precisely, HMS-T gave much sharper hysteresis loop and much higher adsorbed volume than HMS-E. The calculation of adsorption data indicated that HMS-T possessed higher BET surface area and total pore volume (Table 4.4). The pore size distribution shown in Figure 4.14(b) also indicated the larger pore size with narrow distribution for HMS-T. These results should be ascribed to the micelle formation of the organic template in the synthesis media with different properties. The DDA molecules might be dissolved well in THF with lower polarity, leading to stretching of hydrocarbon chain of DDA and expansion of the resultant hexagonal array micelle. The large hysteresis loop at high relative pressure ($P/P_0 > 0.8$) observed for HMS-T should be due to the N_2 condensation in the interparticle voids derived from agglomerates of HMS-T particles. This result suggested that the particle size of HMS-T was smaller than that of HMS-E, as also reflected by higher external surface area for HMS-T (Table 4.4).

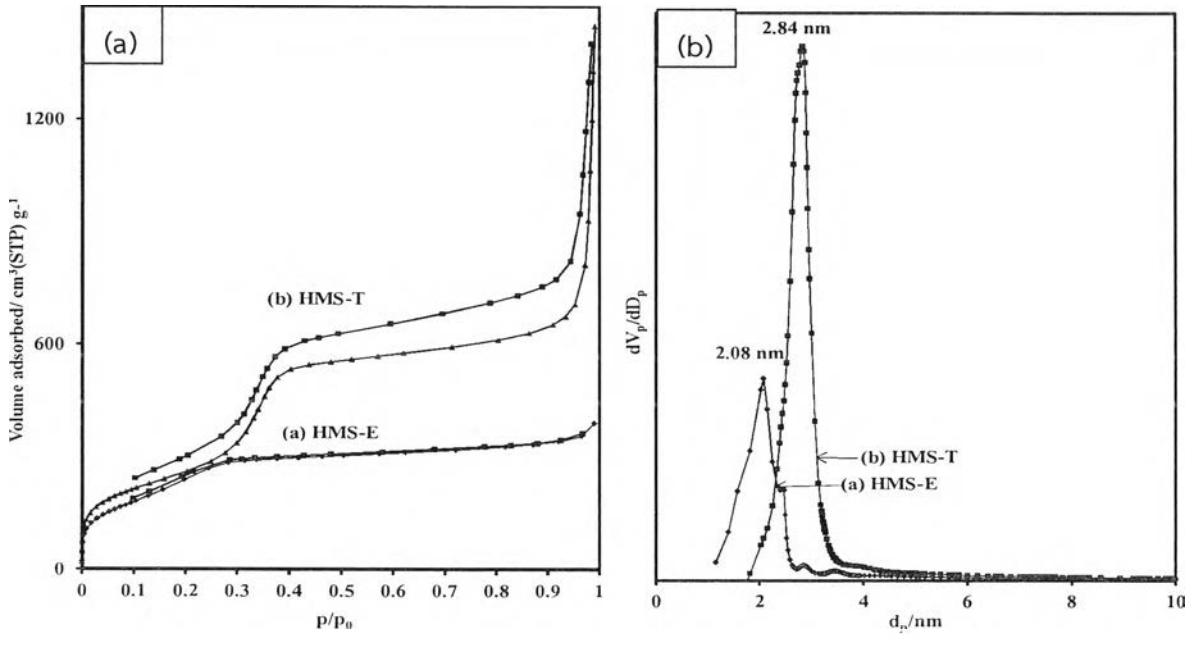

Figure 4.14 N_2 adsorption-desorption isotherms (a) and BJH pore size distribution (b) of pure silica HMS-E and HMS-T.

Table 4.4 Textural properties of pure silica HMS-E and HMS-T.

Sample[a]	Molar composition (mol%)						S_{BET}[b]	S_{ext}[c]	D_p[d]	V_t[e]	V_p[f]
	TEOS	DDA	H_2O	NR	Ethanol	THF	($m^2 g^{-1}$)	($m^2 g^{-1}$)	(nm)	($cm^3 g^{-1}$)	($cm^3 g^{-1}$)
HMS-E	0.1	0.03	2.94	-	0.08	-	917	36	2.1	0.6	0.5
HMS-T	0.1	0.03	2.94	-	-	0.37	955	160	2.8	2.1	0.8

n.d. = not determined.

[a] Extracted samples.

[b] BET specific surface area.

[c] External surface area derived from *t*-plot curves.

[d] Pore diameter, calculated using the BJH method.

[e] Total pore volume.

[f] Mesopore volume, calculated using the BJH method.

The N_2 adsorption-desorption isotherms with type IV were still observed for the NR/HMS composites prepared under various conditions (Figures 4.15(a)–4.17(a)). In comparison with HMS-T, NR/HMS-1 prepared with similar molar composition exhibited lower adsorbed volume and smaller hysteresis loops at P/P_0 of 0.3-0.4 and of > 0.8. From Table 4.5, it can be seen that the BET surface area and total pore volume were decreased, while the pore size of the materials was slightly reduce affected by the addition of NR (Figure 4.15(a)). A part of mesopore channel may be blocked by some NR molecules.

As can be seen from Figure 4.15(a), increasing the amount of H_2O in the synthesis mixtures (from NR/HMS-1 to NR/HMS-3) enhanced the sharpness of hysteresis loop at P/P_0 of 0.3-0.4, whereas the condensation of N_2 in the interparticle voids was decreased (P/P_0 > 0.8). Accordingly, the BET surface area and the primary mesopore volume were increased, while the external surface area was reduced (Table 4.5). Furthermore, the NR/HMS synthesized with high H_2O amount possessed narrower distribution of pore size and enlarged pore diameter (Figure 4.15(b)). The effects of H_2O that resulted in the improvement of the textural properties of the NR/HMS composites could be explained by the silicate-water layer formed during the hydrolysis and condensation of the silica source, which excluded the hydrophobic NR molecules from the mesopore channels and reduced the pore blockage.

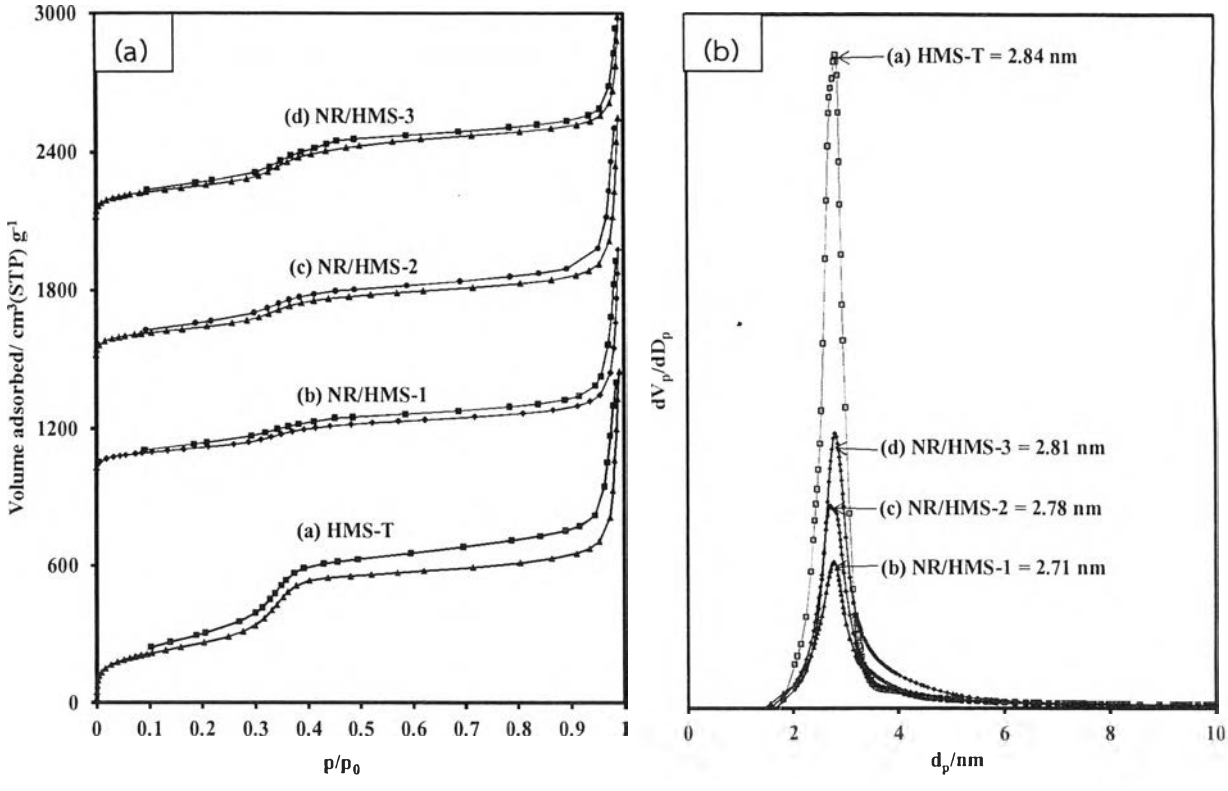

Figure 4.15 N_2 adsorption-desorption isotherms (a) and BJH pore size distribution (b) of pure silica HMS-T and NR/HMS-1 to -3 composites.

Table 4.5 Textural properties of pure silica HMS-T and NR/HMS-1 to -3 composites.

Sample[a]	Molar composition (mol%)					S_{BET}[b]	S_{ext}[c]	D_p[d]	V_t[e]	V_p[f]
	TEOS	DDA	H_2O	NR	THF	($m^2 g^{-1}$)	($m^2 g^{-1}$)	(nm)	($cm^3 g^{-1}$)	($cm^3 g^{-1}$)
HMS-T	0.1	0.03	2.94	-	0.37	955	160	2.8	2.1	0.8
NR/HMS-1	0.1	0.03	2.94	0.01	0.37	428	145	2.7	1.5	0.3
NR/HMS-2	0.1	0.03	4.42	0.01	0.37	514	155	2.8	1.6	0.3
NR/HMS-3	0.1	0.03	5.89	0.01	0.37	571	108	2.8	1.7	0.5

n.d. = not determined.

[a] Extracted samples.

[b] BET specific surface area.

[c] External surface area derived from *t*-plot curves.

[d] Pore diameter, calculated using the BJH method.

[e] Total pore volume.

[f] Mesopore volume, calculated using the BJH method.

Figure 4.16(a) compared the N_2 physisorption isotherms of NR/HMS-4, NR/HMS-5 and NR/HMS-6, all of which were synthesized with different amounts of DDA. The hysteresis loop relating to the primary mesopores (P/P_0 = 0.3-0.4) was increased from NR/HMS-4 to NR/HMS-5, corresponding to higher BET surface area, total pore volume (Table 4.6) and pore size (Figure 4.16(b)). The increased amount of DDA should enhance the complete micelle formation, so that the mesoporosity was improved. However, further increasing the DDA/TEOS ratio to 0.7 (NR/HMS-6) decreased the mesopore volume (Table 4.6) and pore size (Figure 4.16(b)). Interestingly, the NR/HMS composites categorized in this group exhibited large hysteresis loops at P/P_0 > 0.8 (Figure 4.16(a)) as a result of unconventionally high external surface area (Table 4.6). Combining these results with the XRD data suggested the presence of small non-porous silica particles generated at high DDA concentration. The excess DDA molecules may form reverse micelles in which the amine head groups interacted with silica via hydrogen bonding and hydrocarbon tails stretched out to the NR molecules.

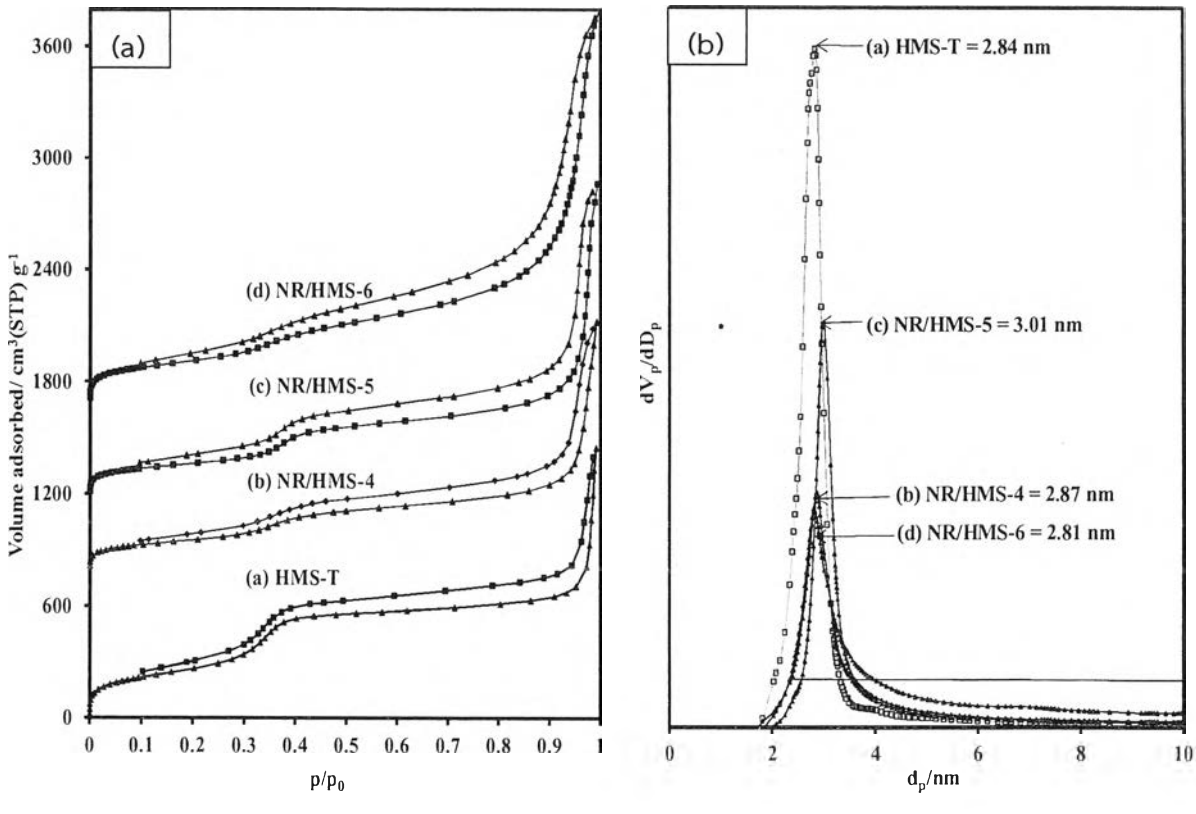

Figure 4.16 N_2 adsorption-desorption isotherms (a) and BJH pore size distribution (b) of pure silica HMS-T and NR/HMS-4 to -6 composites.

Table 4.6 Textural properties of pure silica HMS-T and NR/HMS-4 to -6 composites.

Sample[a]	Molar composition (mol%)					S_{BET}[b] ($m^2 g^{-1}$)	S_{ext}[c] ($m^2 g^{-1}$)	D_p[d] (nm)	V_t[e] ($cm^3 g^{-1}$)	V_p[f] ($cm^3 g^{-1}$)
	TEOS	DDA	H_2O	NR	THF					
HMS-T	0.1	0.03	2.94	-	0.37	955	160	2.8	2.1	0.8
NR/HMS-4	0.1	0.04	2.94	0.01	0.37	562	206	2.9	2.0	0.4
NR/HMS-5	0.1	0.05	2.94	0.01	0.37	594	345	3.0	2.5	0.4
NR/HMS-6	0.1	0.07	2.94	0.01	0.37	768	940	2.8	3.1	0.05

n.d. = not determined.

[a] Extracted samples.

[b] BET specific surface area.

[c] External surface area derived from *t*-plot curves.

[d] Pore diameter, calculated using the BJH method.

[e] Total pore volume.

[f] Mesopore volume, calculated using the BJH method.

The effects of the NR content on the N_2 physisorption isotherm and the textural properties of the composites are included in Figure 4.17(a) and Table 4.7, respectively. The hysteresis loop at P/P_0 between 0.3 and 0.4 observed for NR/HMS-7 was nearly absent when compared to that of NR/HMS-1 (Figure 4.17(a)). The BJH plot indicated that the primary mesopore volume and size were decreased (Figure 4.17(b)). This result suggested an increase in the blockage of mesoporous channels when the higher amount of NR was used. However, NR/HMS-7 exhibited larger hysteresis loop appearing at high relative pressure than NR/HMS-1, corresponding to higher external surface area (Table 4.7). In this case, the agglomeration of the composite particles should be accounted for the sticky nature of NR that covered the outer surface of the silica framework. Therefore, the increase in the total surface area and total pore volume by the higher amount of NR added was derived from the increased textural porosity.

The increase of H_2O amount concomitantly with higher DDA concentration (NR/HMS-8) enhanced the mesoporosity as deduced from the shape of N_2 adsorption-desorption isotherm (Figure 4.17(a)). The BET surface area and the primary mesopore volume of NR/HMS-8 were higher than those of NR/HMS-1 (Table 4.7). Moreover, an enlargement of pore diameter was observed from the BJH plot (Figure 4.17(b)). This result indicated that the NR/HMS composite with good textural and structural properties can be achieved by carefully adjusting the synthesis composition via our developed sol-gel process.

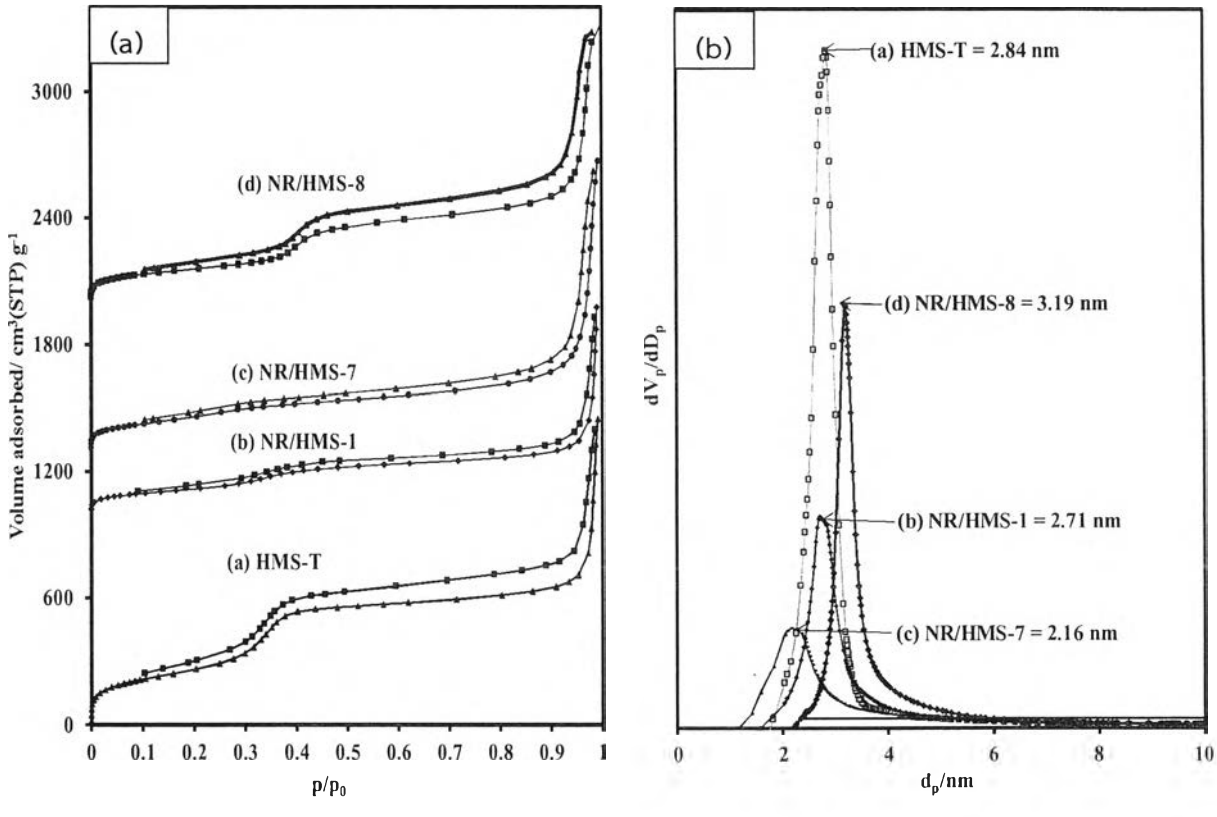

Figure 4.17 N_2 adsorption-desorption isotherms (a) and BJH pore size distribution (b) of pure silica HMS-T and NR/HMS-1, -7 and -8 composites.

Table 4.7 Textural properties of pure silica HMS-T and NR/HMS-1, -7 and -8 composites.

Sample[a]	Molar composition (mol%)					S_{BET}[b]	S_{ext}[c]	D_p[d]	V_t[e]	V_p[f]
	TEOS	DDA	H_2O	NR	THF	($m^2 g^{-1}$)	($m^2 g^{-1}$)	(nm)	($cm^3 g^{-1}$)	($cm^3 g^{-1}$)
HMS-T	0.1	0.03	2.94	-	0.37	955	160	2.8	2.1	0.8
NR/HMS-1	0.1	0.03	2.94	0.01	0.37	428	145	2.7	1.5	0.3
NR/HMS-7	0.1	0.03	2.94	0.02	0.74	598	252	2.2	2.0	0.2
NR/HMS-8	0.1	0.04	5.89	0.01	0.37	570	268	3.2	2.0	0.4

n.d. = not determined.

[a] Extracted samples.

[b] BET specific surface area.

[c] External surface area derived from *t*-plot curves.

[d] Pore diameter, calculated using the BJH method.

[e] Total pore volume.

[f] Mesopore volume, calculated using the BJH method.

4.9 H_2O adsorption-desorption measurement

The technique of H_2O adsorption-desorption measurement was used to evaluate the effects of NR on the hydrophobic properties of the NR/HMS composites. As shown in Figure 4.18, the isotherm of HMS-T was classified to be type IV. The large hysteresis loop and large volume of H_2O adsorbed were related to its high BET surface area, pore diameter and mesopore volume (Table 4.4). The composites of NR/HMS-1 and NR/HMS-3 exhibited similar shape of the isotherm to HMS-T. The smaller primary pore volumes resulted in lower amount of H_2O adsorbed on NR/HMS-1 and NR/HMS-3. The analysis of the adsorption data at low relative pressure indicated a decrease in the monolayer adsorption volume in the following order: HMS-T (59.1 $cm^3 g^{-1}$) > NR/HMS-3 (54.7 $cm^3 g^{-1}$) > NR/HMS-1 (35.8 $cm^3 g^{-1}$). Moreover, the desorption of H_2O condensed in mesopores occurred easier on both NR/HMS composites than the pure silica HMS-T. These results should be due to the depletion of surface silanol groups by the NR molecules coverage as suggested by the FTIR and ^{29}Si MAS NMR results (Figures 4.3 and 4.4, respectively).

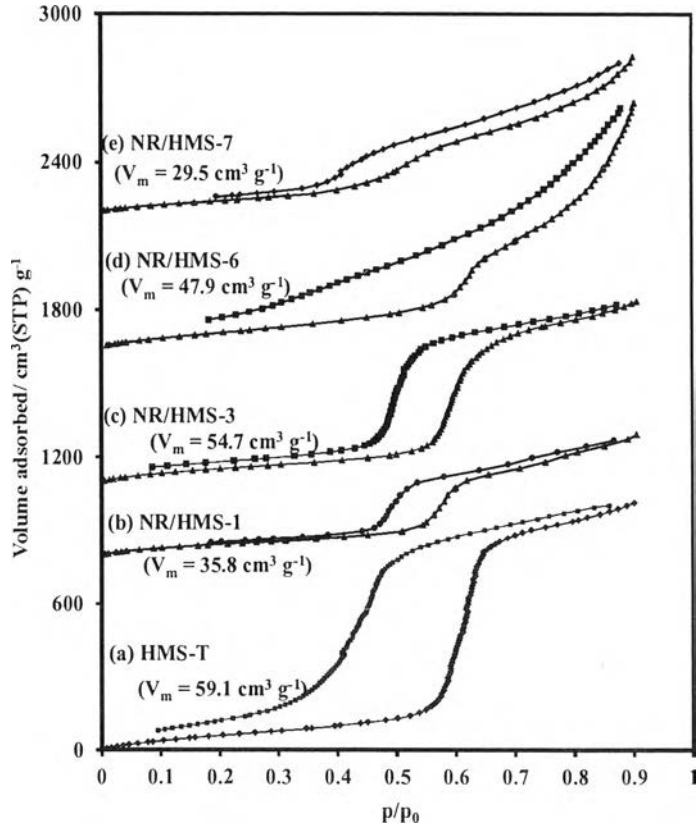

Figure 4.18 H_2O adsorption-desorption isotherms of HMS-T and NR/HMS composites.

The H_2O adsorption-desorption isotherms attained from NR/HMS-7 with high NR loading and NR/HMS-6 synthesized with high DDA/TEOS ratio showed alterative type relating to the materials weakly interacting with the adsorbate [102]. Taking into account their adsorption branch, there was two-step uptake of H_2O presenting at medium and high relative pressures, in which the former step was the adsorption of H_2O in the primary mesopores and the latter step was derived from H_2O filled in the interparticle voids. The desorption of H_2O from NR/HMS-6 and NR/HMS-7 gradually occurred probably due to the large hydrophobic external surface area and textural pore volume of both composites (Table 4.6 and 4.7). The volume of H_2O adsorbed monolayer on NR/HMS-6 and NR/HMS-7 were 47.9 and 29.5 $cm^3 g^{-1}$, respectively.

4.10 Pathway for the formation of NR/HMS composite.

According to the study in this chapter, the postulated mechanism for formation of NR/HMS composites occurred via the sol-gel process is depicted in Figure 4.19. Firstly, TEOS and DDA are homogeneously dissolved in the NR solution using THF as the synthesis media. Upon adding H_2O, TEOS is hydrolyzed to silicate species simultaneously with the rearrangement of DDA molecules into isolated rod-like micelles induced by hydrogen-bonding between the amine and the silicate hydroxyl groups. Further condensation of the silicate species results in silicate aggregates encapsulating the micellar rods that randomly order into a hexagonal assembly. H_2O and ethanol produced around the silicate walls form hydrophilic layer and exclude the NR molecules to outer surface at which the silicate rods are loosely packing. After the precipitation of the slurry in ethanol by which THF solvent is removed, the NR molecules are condensed and packed inside the hexagonal silica arrays. Although the NR/HMS series had inferior the BET surface area and the mesopore volume to the pure silica HMS, the composites may take advantages of the higher external surface area, higher textural pore volume and larger pore size.

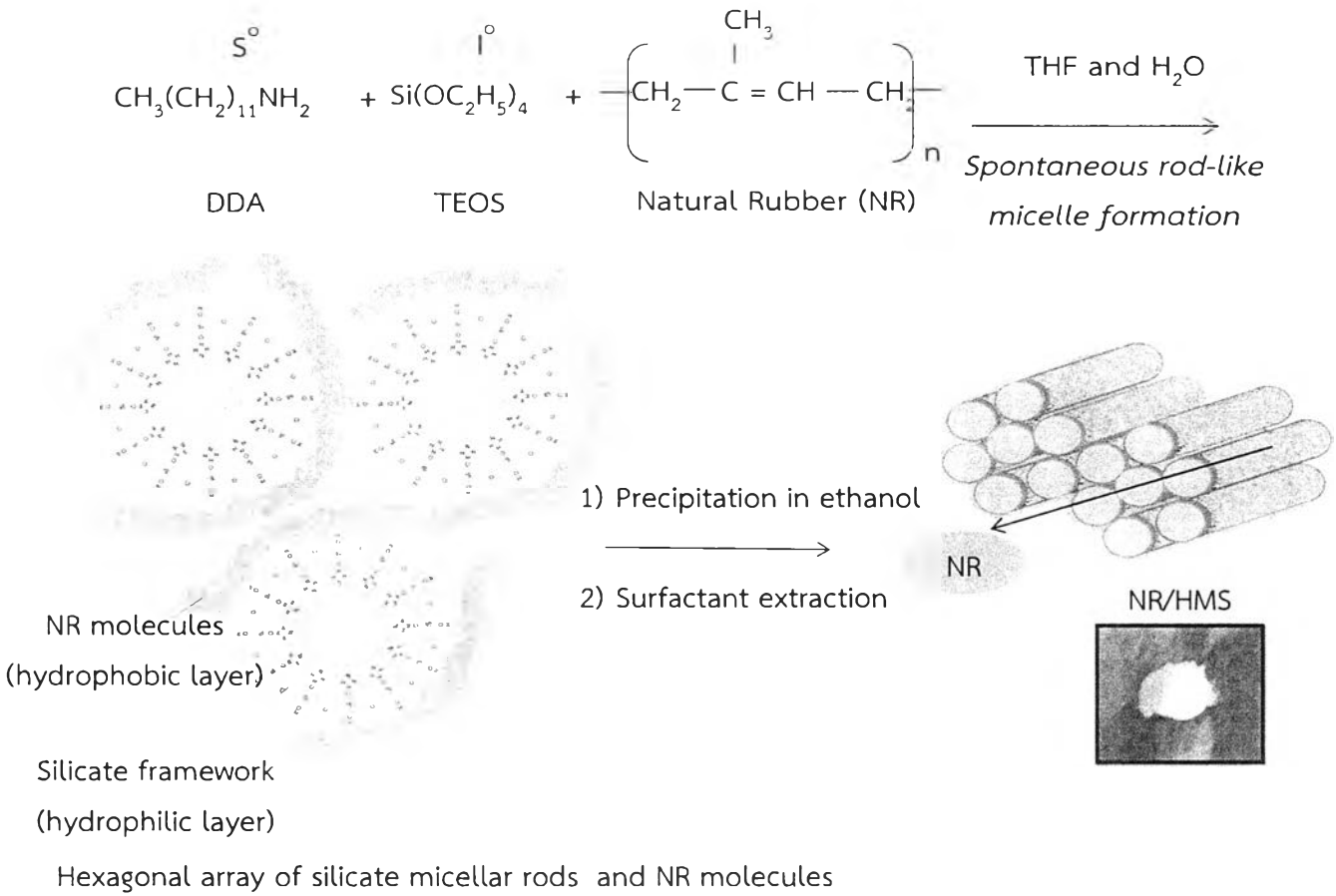

Figure 4.19 Pathway for the formation of NR/HMS composite.